Electronic supplementary information

High-throughput design of complex oxides as isothermal, redox-activated CO_2 sorbents for hydrogen generation

Runxia Cai,‡[a] Kunran Yang,‡[a] Xijun Wang,‡[a,b] Mahe Rukh,[a] Azin Saberi Bosari,[a] Eric Giavedoni,[a] Alexandra Pierce,[a] Leo Brody,[a] Wentao Tang,[a] Phillip R. Westmoreland,[a] Fanxing Li*[a]

[a] *Department of Chemical and Biomolecular Engineering, North Carolina State University, 911 Partners Way, Raleigh, North Carolina 27695-7905, USA*

[b] *Department of Chemical and Biological Engineering, Northwestern University, Evanston, Illinois 60208, USA*

‡ *These authors contributed equally to this work*

**Corresponding author, fli5@ncsu.edu*

1. **Table S1.** The perovskite PTSs tested in this study

Sample number	Sample Name	Ball milling time and calcination temperature	XRD	CO_2 capacity (%)
1	$Sr_{0.625}Ba_{0.375}Fe_{0.75}Co_{0.25}O_{3-\delta}$	24 h, 1000℃	Pure	25.27
2	$Sr_{0.5}Ba_{0.5}Fe_{0.75}Co_{0.25}O_{3-\delta}$	24 h, 1000 ℃	Pure	25.02
3	$Sr_{0.375}Ba_{0.625}Fe_{0.75}Co_{0.25}O_{3-\delta}$	24 h, 1000 ℃	Pure	29.43
4	$Sr_{0.25}Ba_{0.75}Fe_{0.75}Co_{0.25}O_{3-\delta}$	3 h, 1000 ℃	Pure	26.61
5	$Sr_{0.625}Ba_{0.375}Fe_{0.375}Co_{0.625}O_{3-\delta}$	3 h, 1000 ℃	Pure	46.18
6	$Sr_{0.5}Ba_{0.5}Fe_{0.375}Co_{0.625}O_{3-\delta}$	3 h, 1000 ℃	Pure	44.45
7	$Sr_{0.375}Ba_{0.625}Fe_{0.375}Co_{0.625}O_{3-\delta}$	24 h, 1000 ℃	Pure	42.10
8	$Sr_{0.25}Ba_{0.75}Fe_{0.375}Co_{0.625}O_{3-\delta}$	24 h, 1000 ℃	Pure	46.61
9	$Sr_{0.625}Ba_{0.375}Fe_{0.5}Co_{0.5}O_{3-\delta}$	24 h, 1000 ℃	Pure	49.44
10	$Sr_{0.375}Ba_{0.625}Fe_{0.5}Co_{0.5}O_{3-\delta}$	24 h, 1000 ℃	Pure	28.26
11	$Sr_{0.625}Ba_{0.375}Fe_{0.25}Co_{0.75}O_{3-\delta}$	24 h, 1000 ℃	Pure	48.85
12	$Sr_{0.5}Ba_{0.5}Fe_{0.25}Co_{0.75}O_{3-\delta}$	24 h, 1000 ℃	Pure	48.59
13	$Sr_{0.375}Ba_{0.625}Fe_{0.25}Co_{0.75}O_{3-\delta}$	24 h, 1000 ℃	Pure	42.80
14	$Sr_{0.25}Ba_{0.75}Fe_{0.25}Co_{0.75}O_{3-\delta}$	24 h, 1000 ℃	Pure	34.03
15	$Sr_{0.25}Ba_{0.75}Fe_{0.5}Co_{0.5}O_{3-\delta}$	24 h, 1000 ℃	Pure	17.89
16	$Sr_{0.125}Ba_{0.875}Fe_{0.75}Co_{0.25}O_{3-\delta}$	24 h, 1000 ℃	Nearly pure	17.24
17	$Sr_{0.125}Ba_{0.875}Fe_{0.5}Co_{0.5}O_{3-\delta}$	24 h, 1000 ℃	Pure	20.14
18	$Sr_{0.5}Ba_{0.5}Fe_{0.5}Co_{0.5}O_{3-\delta}$	3 h, 1000 ℃	Pure	29.88
19	$Sr_{0.625}Ba_{0.375}Fe_{0.875}Co_{0.125}O_{3-\delta}$	24 h, 1000 ℃	Pure	10.65
20	$Sr_{0.5}Ba_{0.5}Fe_{0.875}Co_{0.125}O_{3-\delta}$	3 h, 1000 ℃	Pure	11.87
21	$Sr_{0.375}Ba_{0.625}Fe_{0.875}Co_{0.125}O_{3-\delta}$	24 h, 1000 ℃	Pure	10.56
22	$Sr_{0.25}Ba_{0.75}Fe_{0.875}Co_{0.125}O_{3-\delta}$	3 h, 1000 ℃	Pure	14.64
23	$Sr_{0.875}Ca_{0.125}Fe_{0.125}Co_{0.875}O_{3-\delta}$	3 h, 1000 ℃	pure	15.17
24	$Sr_{0.75}Ca_{0.25}Fe_{0.125}Co_{0.875}O_{3-\delta}$	3 h, 1000 ℃	Pure	13.80
25	$Sr_{0.875}Ca_{0.125}Fe_{0.25}Co_{0.75}O_{3-\delta}$	3 h, 1000 ℃	Pure	4.97
26	$Sr_{0.75}Ca_{0.25}Fe_{0.25}Co_{0.75}O_{3-\delta}$	3 h, 1000 ℃	Pure	9.39
27	$Sr_{0.25}Ba_{0.75}Fe_{0.875}Ni_{0.125}O_{3-\delta}$	3 h, 1000 ℃	Pure	13.40
28	$Sr_{0.375}Ba_{0.625}Fe_{0.875}Ni_{0.125}O_{3-\delta}$	3 h, 1000 ℃	Pure	12.21
29	$Sr_{0.5}Ba_{0.5}Fe_{0.875}Ni_{0.125}O_{3-\delta}$	3 h, 1000 ℃	Pure	10.33
30	$Sr_{0.625}Ba_{0.375}Fe_{0.875}Ni_{0.125}O_{3-\delta}$	3 h, 1000 ℃	Pure	9.13
31	$Sr_{0.875}Ca_{0.125}Fe_{0.375}Co_{0.625}O_{3-\delta}$	3 h, 1000 ℃	Pure	2.94
32	$Sr_{0.75}Ca_{0.25}Fe_{0.375}Co_{0.625}O_{3-\delta}$	3 h, 1000 ℃	Pure	2.66
33	$Sr_{0.625}Ca_{0.375}Fe_{0.125}Co_{0.875}O_{3-\delta}$	3 h, 1000 ℃	Pure	15.96
34	$Sr_{0.625}Ca_{0.375}Fe_{0.25}Co_{0.75}O_{3-\delta}$	3 h, 1000 ℃	Pure	13.94
35	$Sr_{0.25}Ba_{0.75}Fe_{0.75}Ni_{0.25}O_{3-\delta}$	3 h, 1000 ℃	Impure	-
36	$Sr_{0.375}Ba_{0.625}Fe_{0.75}Ni_{0.25}O_{3-\delta}$	3 h, 1000 ℃	Impure	-
37	$Sr_{0.5}Ba_{0.5}Fe_{0.75}Ni_{0.25}O_{3-\delta}$	3 h, 1000 ℃	Impure	-

38	$Sr_{0.625}Ba_{0.375}Fe_{0.75}Ni_{0.25}O_{3-\delta}$	3 h, 1000 °C	Impure	-
39	$Sr_{0.875}Ca_{0.125}Fe_{0.125}Mn_{0.875}O_{3-\delta}$	3 h, 1200 °C	Nearly pure	53.36
40	$Sr_{0.875}Ca_{0.125}Fe_{0.25}Mn_{0.75}O_{3-\delta}$	3 h, 1200 °C	Nearly pure	27.41
41	$SrCaFe_{0.125}Mn_{0.875}O_{3-\delta}$	3 h, 1200 °C	Nearly pure	59.36
42	$SrFe_{0.25}Mn_{0.75}O_{3-\delta}$	3 h, 1200 °C	Nearly pure	21.19
43	$Sr_{0.25}Ba_{0.75}Fe_{0.75}Mn_{0.25}O_{3-\delta}$	3 h, 1000 °C	Impure	-
44	$Sr_{0.375}Ba_{0.625}Fe_{0.75}Mn_{0.25}O_{3-\delta}$	3 h, 1000 °C	Impure	-
45	$Sr_{0.5}Ba_{0.5}Fe_{0.75}Mn_{0.25}O_{3-\delta}$	3 h, 1000 °C	Impure	-
46	$Sr_{0.625}Ba_{0.375}Fe_{0.75}Mn_{0.25}O_{3-\delta}$	3 h, 1000 °C	Impure	-
47	$Sr_{0.375}Ba_{0.625}Fe_{0.875}Cu_{0.125}O_{3-\delta}$	3 h, 1000 °C	Pure	1.23
48	$Sr_{0.5}Ba_{0.5}Fe_{0.875}Cu_{0.125}O_{3-\delta}$	3 h, 1000 °C	Pure	1.98
49	$Sr_{0.625}Ba_{0.375}Fe_{0.875}Cu_{0.125}O_{3-\delta}$	3 h, 1000 °C	Pure	1.46
50	$Sr_{0.25}Ba_{0.75}Fe_{0.875}Cu_{0.125}O_{3-\delta}$	3 h, 1000 °C	Pure	1.14
51	$Sr_{0.875}K_{0.125}Fe_{0.375}Co_{0.625}O_{3-\delta}$	3 h, 1000 °C	Pure	7.84
52	$Sr_{0.875}K_{0.125}Fe_{0.5}Co_{0.5}O_{3-\delta}$	3 h, 1000 °C	Pure	1.13
53	$Sr_{0.875}K_{0.125}Fe_{0.625}Co_{0.375}O_{3-\delta}$	3 h, 1000 °C	Pure	0.91
54	$Sr_{0.875}K_{0.125}Fe_{0.875}Mn_{0.125}O_{3-\delta}$	3 h, 1000 °C	Pure	1.47
55	$Sr_{0.875}K_{0.125}Fe_{0.625}Mn_{0.375}O_{3-\delta}$	3 h, 1000 °C	Pure	4.87
56	$Sr_{0.875}K_{0.125}Fe_{0.5}Mn_{0.5}O_{3-\delta}$	3 h, 1000 °C	Pure	4.60
57	$Sr_{0.875}K_{0.125}Fe_{0.375}Mn_{0.625}O_{3-\delta}$	3 h, 1000 °C	Impure	-
58	$Sr_{0.875}Ca_{0.125}MnO_{3-\delta}$	3 h, 1000 °C	Pure	39.76
59	$SrMnO_{3-\delta}$	3 h, 1200 °C	Pure	75.36
60	$Sr_{0.75}Ca_{0.25}Fe_{0.125}Mn_{0.875}O_{3-\delta}$	3 h, 1200 °C	Nearly pure	39.10
61	$Sr_{0.75}Ca_{0.25}Fe_{0.25}Mn_{0.75}O_{3-\delta}$	3 h, 1200 °C	Nearly pure	20.34
62	$Sr_{0.25}Ba_{0.75}Fe_{0.875}Mn_{0.125}O_{3-\delta}$	3 h, 1000 °C	Impure	
63	$Sr_{0.375}Ba_{0.625}Fe_{0.875}Mn_{0.125}O_{3-\delta}$	3 h, 1000 °C	Impure	
64	$Sr_{0.5}Ba_{0.5}Fe_{0.875}Mn_{0.125}O_{3-\delta}$	3 h, 1000 °C	Nearly pure	5.35
65	$Sr_{0.625}Ba_{0.375}Fe_{0.875}Mn_{0.125}O_{3-\delta}$	3 h, 1000 °C	Nearly pure	4.23
66	$SrFeO_{3-\delta}$	3 h, 1000 °C	Pure	0.17
67	$BaFeO_{3-\delta}$	3 h, 1000 °C	Impure	-
68	$BaMnO_{3-\delta}$	3 h, 1000 °C	Pure	76.58
69	$Sr_{0.75}Ba_{0.25}Fe_{0.875}Mn_{0.125}O_{3-\delta}$	3 h, 1000 °C	Pure	9.33
70	$Sr_{0.625}Ba_{0.375}Fe_{0.125}Co_{0.875}O_{3-\delta}$	3 h, 1000 °C	Pure	38.48
71	$Sr_{0.5}Ba_{0.5}Fe_{0.125}Co_{0.875}O_{3-\delta}$	3 h, 1000 °C	Pure	40.67
72	$Sr_{0.375}Ba_{0.625}Fe_{0.125}Co_{0.875}O_{3-\delta}$	3 h, 1000 °C	Pure	30.30
73	$Sr_{0.25}Ba_{0.75}Fe_{0.125}Co_{0.875}O_{3-\delta}$	3 h, 1000 °C	Impure	-
74	$Sr_{0.875}Ba_{0.125}FeO_{3-\delta}$	3 h, 1000 °C	Pure	0.22
75	$Sr_{0.75}Ba_{0.25}FeO_{3-\delta}$	3 h, 1000 °C	Pure	0.24
76	$Sr_{0.625}Ba_{0.375}FeO_{3-\delta}$	3 h, 1000 °C	Pure	0.22
77	$SrFe_{0.375}Mn_{0.625}O_{3-\delta}$	3 h, 1000 °C	Pure	8.64
78	$SrFe_{0.875}Mg_{0.125}O_{3-\delta}$	3 h, 1000 °C	Nearly pure	1.97

79	$Sr_{0.875}Ba_{0.125}Fe_{0.875}Mg_{0.125}O_{3-\delta}$	3 h, 1000 °C	Nearly Pure	1.12
80	$Sr_{0.75}Ba_{0.25}Fe_{0.875}Mg_{0.125}O_{3-\delta}$	3 h, 1000 °C	Nearly pure	2.14
81	$Sr_{0.625}Ba_{0.375}Fe_{0.875}Mg_{0.125}O_{3-\delta}$	3 h, 1000 °C	Nearly pure	6.80
82	$SrCoO_{3-\delta}$	3 h, 1000 °C	Pure	39.97
83	$SrFe_{0.125}Co_{0.875}O_{3-\delta}$	3 h, 1000 °C	Pure	18.50
84	$SrFe_{0.25}Co_{0.75}O_{3-\delta}$	3 h, 1000 °C	Pure	15.09
85	$Sr_{0.875}Ca_{0.125}CoO_{3-\delta}$	3 h, 1000 °C	Pure	36.62
86	$Sr_{0.875}Ca_{0.125}Fe_{0.875}Co_{0.125}O_{3-\delta}$	3 h, 1000 °C	Pure	2.68
87	$Sr_{0.75}Ca_{0.25}Fe_{0.875}Co_{0.125}\ O_{3-\delta}$	3 h, 1000 °C	Pure	2.03
88	$Sr_{0.875}Ca_{0.125}Fe_{0.75}Co_{0.25}\ O_{3-\delta}$	3 h, 1000 °C	Pure	0.12
89	$Sr_{0.75}Ca_{0.25}Fe_{0.75}Co_{0.25}O_{3-\delta}$	3 h, 1000 °C	Pure	0.39
90	$Sr_{0.75}Ca_{0.25}Fe_{0.875}Ni_{0.125}O_{3-\delta}$	3 h, 1000 °C	Impure	-
91	$Sr_{0.625}Ca_{0.375}Fe_{0.875}Ni_{0.125}O_{3-\delta}$	3 h, 1000 °C	Impure	-
92	$Sr_{0.5}Ca_{0.5}Fe_{0.875}Ni_{0.125}O_{3-\delta}$	3 h, 1000 °C	Nearly pure	0.77
93	$Sr_{0.375}Ca_{0.625}Fe_{0.875}Ni_{0.125}O_{3-\delta}$	3 h, 1000 °C	Nearly pure	0.24
94	$Sr_{0.75}Ca_{0.25}Fe_{0.875}Mg_{0.125}O_{3-\delta}$	3 h, 1000 °C	Nearly pure	0.91
95	$Sr_{0.625}Ca_{0.375}Fe_{0.875}Mg_{0.125}O_{3-\delta}$	3 h, 1000 °C	Nearly pure	0.52
96	$Sr_{0.5}Ca_{0.5}Fe_{0.875}Mg_{0.125}O_{3-\delta}$	3 h, 1000 °C	Pure	0.48
97	$Sr_{0.375}Ca_{0.625}Fe_{0.875}Mg_{0.125}O_{3-\delta}$	3 h, 1000 °C	Pure	0.39
98	$Sr_{0.875}Ba_{0.125}MnO_{3-\delta}$	3 h, 1200 °C	Pure	66.18
99	$Sr_{0.75}Ba_{0.25}MnO_{3-\delta}$	3 h, 1200 °C	Pure	77.85
100	$Sr_{0.625}Ba_{0.375}MnO_{3-\delta}$	3 h, 1200 °C	Nearly pure	68.59

2. Heatmaps of remaining perovskite structures passing each screened step

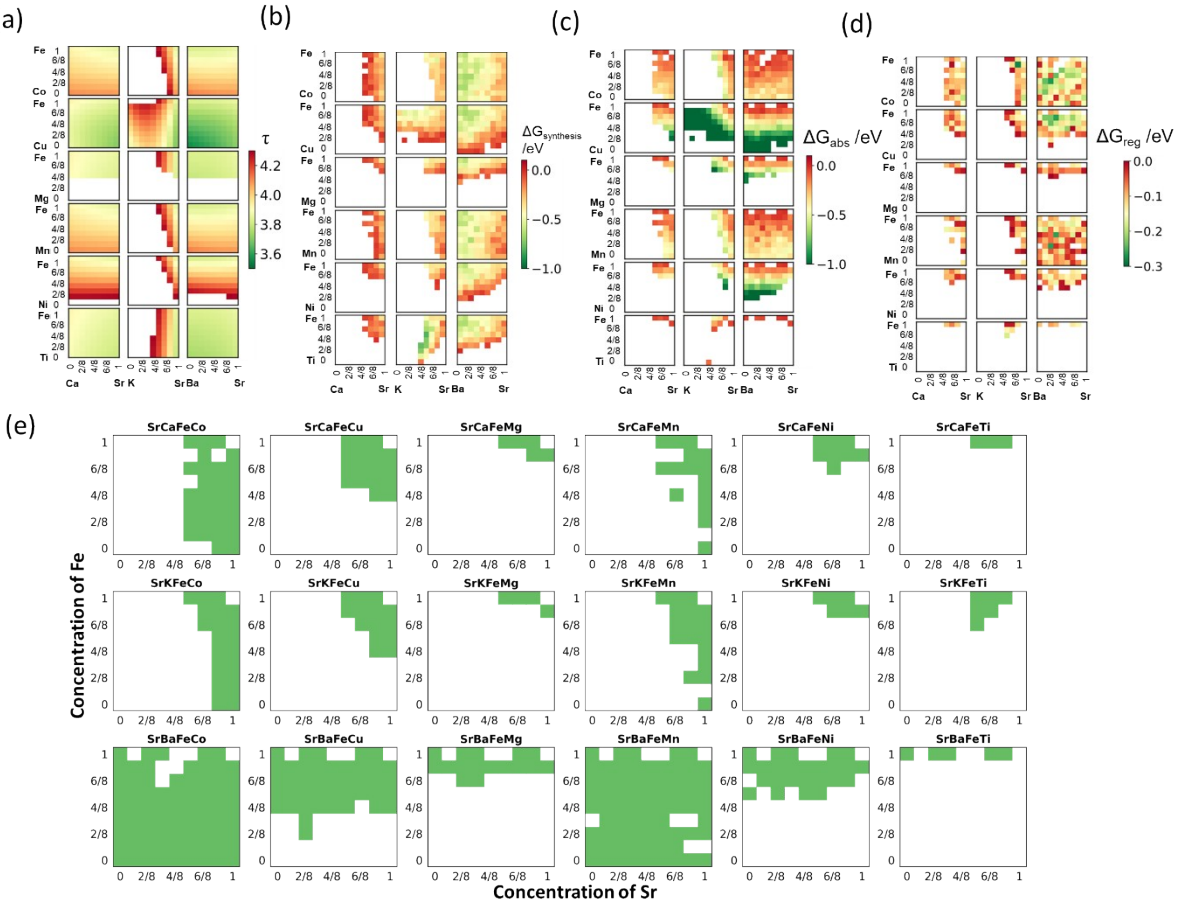

Figure S1. Heatmaps of remaining perovskite structures passing each screened step. (a) τ after modified tolerance factor screening ($\tau \leq 4.3$); (b) $\Delta G_{synthesis}$ after the screening step of (a) and the screening of synthesis process ($\Delta G_{synthesis} \leq 0$ eV); (c) ΔG_{abs} after the screening step of (b) and the reduction and carbonation process under H_2 and CO_2 condition ($\Delta G_{abs} \leq 0$ eV); (d) ΔG_{reg} after the screening step of (c) and the regeneration of the crystal structure under O_2 condition ($\Delta G_{reg} \leq 0$ eV); The color bars are shown respectively to indicate the values. (e) the final screened structure composition. Green areas indicate the materials that pass all the criteria. The x and y axes denote the concentration of Sr and Fe of $Sr_xA_{1-x}Fe_yB_{1-y}O_{3-\delta}$ composition, respectively. For example, when x=2/8 and y=3/8 for SrBaFeCu composition, it means the $Sr_{0.25}Ba_{0.75}Fe_{0.375}Cu_{0.625}O_{3-\delta}$ structure

3. **Figure S2.** XRD patterns of the samples screened

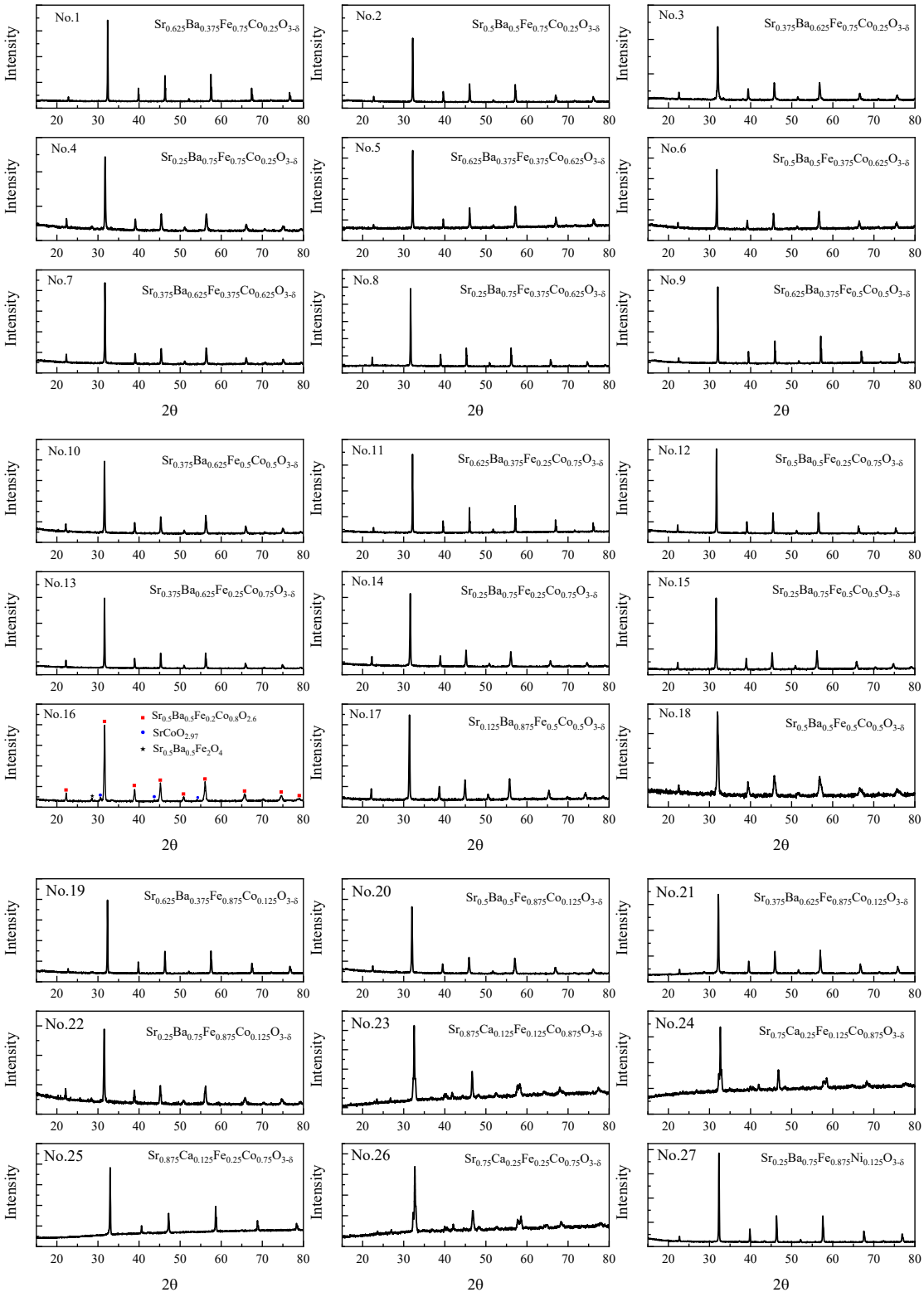

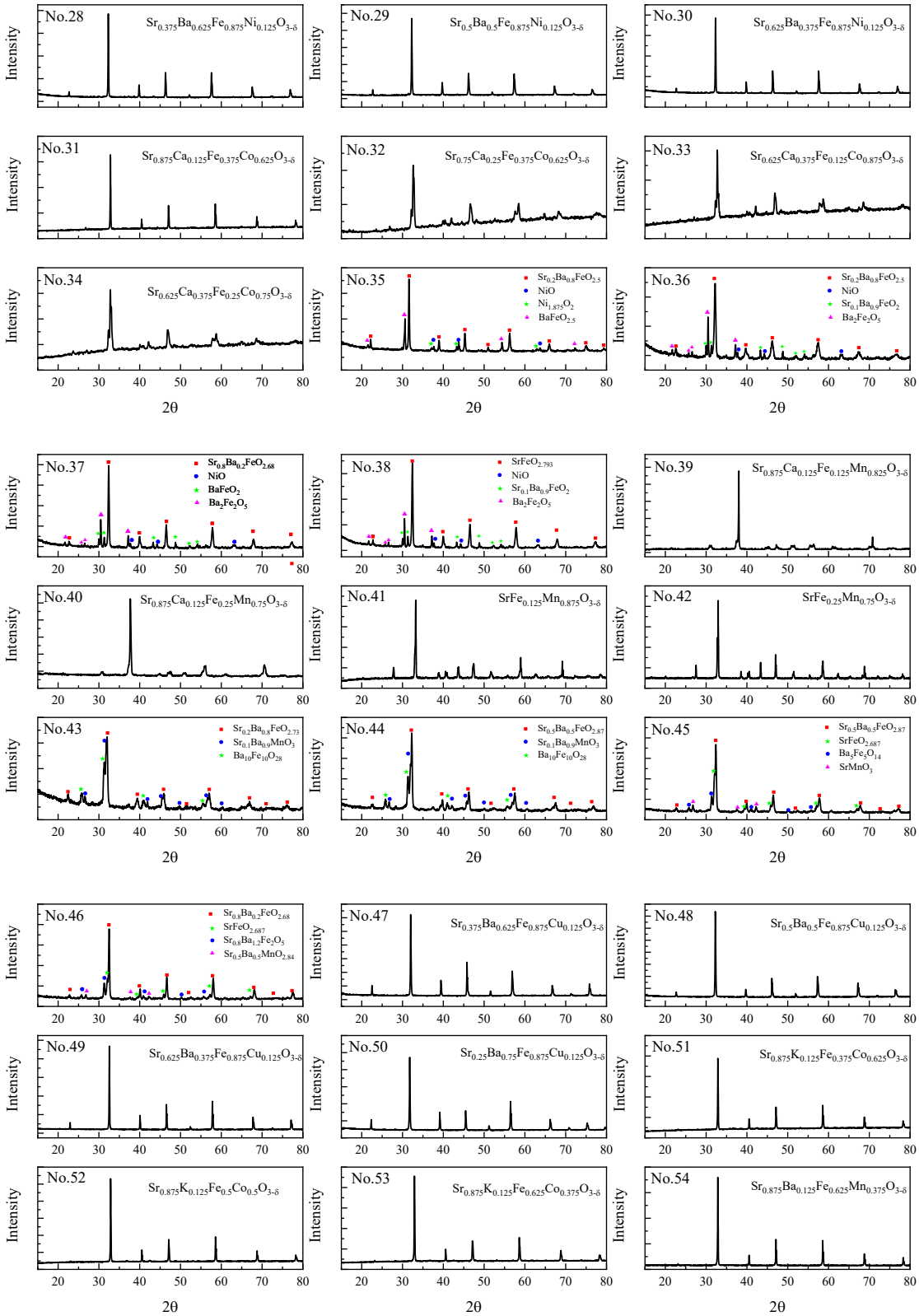
No.28
$Sr_{0.375}Ba_{0.625}Fe_{0.875}Ni_{0.125}O_{3-\delta}$
No.29
$Sr_{0.5}Ba_{0.5}Fe_{0.875}Ni_{0.125}O_{3-\delta}$
No.30
$Sr_{0.625}Ba_{0.375}Fe_{0.875}Ni_{0.125}O_{3-\delta}$
No.31
$Sr_{0.875}Ca_{0.125}Fe_{0.375}Co_{0.625}O_{3-\delta}$
No.32
$Sr_{0.75}Ca_{0.25}Fe_{0.375}Co_{0.625}O_{3-\delta}$
No.33
$Sr_{0.625}Ca_{0.375}Fe_{0.125}Co_{0.875}O_{3-\delta}$
No.34
$Sr_{0.625}Ca_{0.375}Fe_{0.25}Co_{0.75}O_{3-\delta}$
No.35
$Sr_{0.2}Ba_{0.8}FeO_{2.5}$
NiO
$Ni_{1.875}O_2$
$BaFeO_{2.5}$
No.36
$Sr_{0.2}Ba_{0.8}FeO_{2.5}$
NiO
$Sr_{0.1}Ba_{0.9}FeO_2$
$Ba_2Fe_2O_5$
No.37
$Sr_{0.8}Ba_{0.2}FeO_{2.68}$
NiO
$BaFeO_2$
$Ba_2Fe_2O_5$
No.38
$SrFeO_{2.793}$
NiO
$Sr_{0.1}Ba_{0.9}FeO_2$
$Ba_2Fe_2O_5$
No.39
$Sr_{0.875}Ca_{0.125}Fe_{0.125}Mn_{0.825}O_{3-\delta}$
No.40
$Sr_{0.875}Ca_{0.125}Fe_{0.25}Mn_{0.75}O_{3-\delta}$
No.41
$SrFe_{0.125}Mn_{0.875}O_{3-\delta}$
No.42
$SrFe_{0.25}Mn_{0.75}O_{3-\delta}$
No.43
$Sr_{0.2}Ba_{0.8}FeO_{2.73}$
$Sr_{0.1}Ba_{0.9}MnO_3$
$Ba_{10}Fe_{10}O_{28}$
No.44
$Sr_{0.5}Ba_{0.5}FeO_{2.87}$
$Sr_{0.1}Ba_{0.9}MnO_3$
$Ba_{10}Fe_{10}O_{28}$
No.45
$Sr_{0.5}Ba_{0.5}FeO_{2.87}$
$SrFeO_{2.687}$
$Ba_2Fe_2O_{14}$
$SrMnO_3$
No.46
$Sr_{0.8}Ba_{0.2}FeO_{2.68}$
$SrFeO_{2.687}$
$Sr_{0.8}Ba_{1.2}Fe_2O_5$
$Sr_{0.5}Ba_{0.5}MnO_{2.84}$
No.47
$Sr_{0.375}Ba_{0.625}Fe_{0.875}Cu_{0.125}O_{3-\delta}$
No.48
$Sr_{0.5}Ba_{0.5}Fe_{0.875}Cu_{0.125}O_{3-\delta}$
No.49
$Sr_{0.625}Ba_{0.375}Fe_{0.875}Cu_{0.125}O_{3-\delta}$
No.50
$Sr_{0.25}Ba_{0.75}Fe_{0.875}Cu_{0.125}O_{3-\delta}$
No.51
$Sr_{0.875}K_{0.125}Fe_{0.375}Co_{0.625}O_{3-\delta}$
No.52
$Sr_{0.875}K_{0.125}Fe_{0.5}Co_{0.5}O_{3-\delta}$
No.53
$Sr_{0.875}K_{0.125}Fe_{0.625}Co_{0.375}O_{3-\delta}$
No.54
$Sr_{0.875}Ba_{0.125}Fe_{0.625}Mn_{0.375}O_{3-\delta}$
Intensity
2θ
20
30
40
50
60
70
80

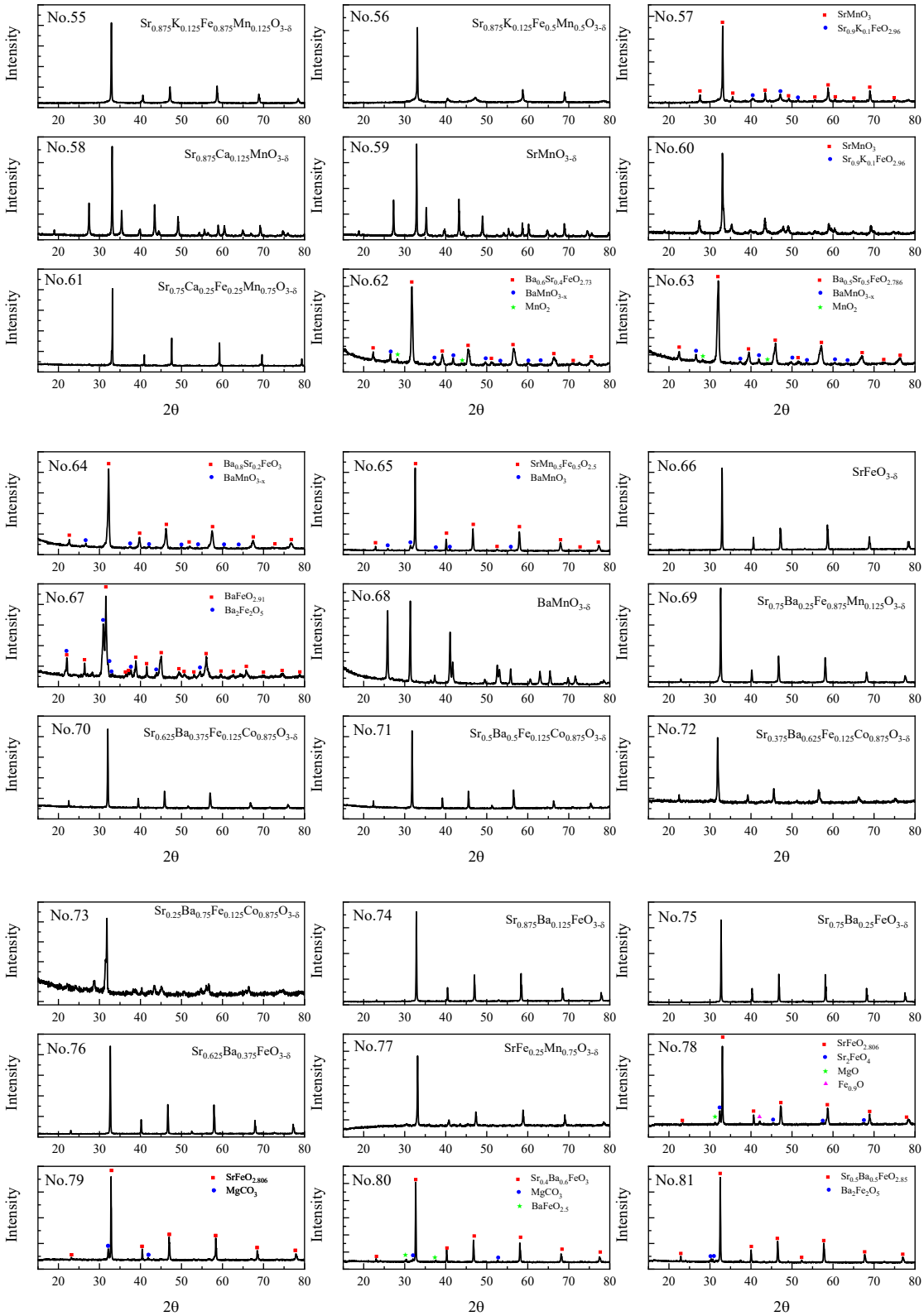
No.55
$Sr_{0.875}K_{0.125}Fe_{0.875}Mn_{0.125}O_{3-\delta}$
No.56
$Sr_{0.875}K_{0.125}Fe_{0.5}Mn_{0.5}O_{3-\delta}$
No.57
$SrMnO_3$
$Sr_{0.9}K_{0.1}FeO_{2.96}$
No.58
$Sr_{0.875}Ca_{0.125}MnO_{3-\delta}$
No.59
$SrMnO_{3-\delta}$
No.60
$SrMnO_3$
$Sr_{0.9}K_{0.1}FeO_{2.96}$
No.61
$Sr_{0.75}Ca_{0.25}Fe_{0.25}Mn_{0.75}O_{3-\delta}$
No.62
$Ba_{0.6}Sr_{0.4}FeO_{2.73}$
$BaMnO_{3-x}$
MnO_2
No.63
$Ba_{0.5}Sr_{0.5}FeO_{2.786}$
$BaMnO_{3-x}$
MnO_2
No.64
$Ba_{0.8}Sr_{0.2}FeO_3$
$BaMnO_{3-x}$
No.65
$SrMn_{0.5}Fe_{0.5}O_{2.5}$
$BaMnO_3$
No.66
$SrFeO_{3-\delta}$
No.67
$BaFeO_{2.91}$
$Ba_2Fe_2O_5$
No.68
$BaMnO_{3-\delta}$
No.69
$Sr_{0.75}Ba_{0.25}Fe_{0.875}Mn_{0.125}O_{3-\delta}$
No.70
$Sr_{0.625}Ba_{0.375}Fe_{0.125}Co_{0.875}O_{3-\delta}$
No.71
$Sr_{0.5}Ba_{0.5}Fe_{0.125}Co_{0.875}O_{3-\delta}$
No.72
$Sr_{0.375}Ba_{0.625}Fe_{0.125}Co_{0.875}O_{3-\delta}$
No.73
$Sr_{0.25}Ba_{0.75}Fe_{0.125}Co_{0.875}O_{3-\delta}$
No.74
$Sr_{0.875}Ba_{0.125}FeO_{3-\delta}$
No.75
$Sr_{0.75}Ba_{0.25}FeO_{3-\delta}$
No.76
$Sr_{0.625}Ba_{0.375}FeO_{3-\delta}$
No.77
$SrFe_{0.25}Mn_{0.75}O_{3-\delta}$
No.78
$SrFeO_{2.806}$
Sr_2FeO_4
MgO
$Fe_{0.9}O$
No.79
$SrFeO_{2.806}$
$MgCO_3$
No.80
$Sr_{0.4}Ba_{0.6}FeO_3$
$MgCO_3$
$BaFeO_{2.5}$
No.81
$Sr_{0.5}Ba_{0.5}FeO_{2.85}$
$Ba_2Fe_2O_5$
Intensity
2θ
20
30
40
50
60
70
80

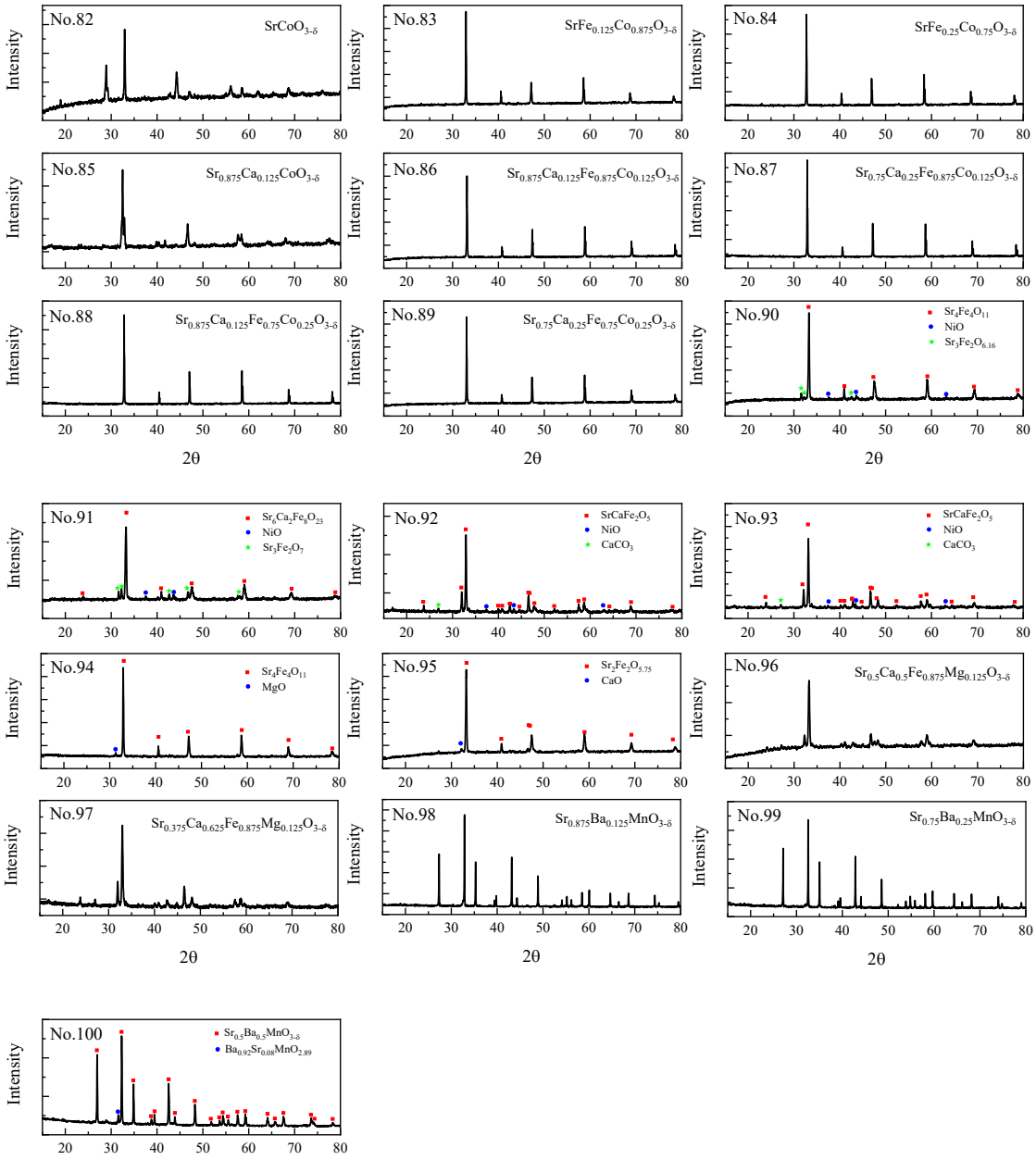

Figure S2. XRD patterns of the samples screened

4. Additional comparison results between DFT simulation and experimental measurement

Considering the significant influence of A-site and B-site dopants on the sorption capacities of $Sr_xBa_{1-x}Fe_yCo_{1-y}O_{3-\delta}$ and $Sr_xBa_{1-x}Fe_yMn_{1-y}O_{3-\delta}$ perovskites, we conducted a more detailed fitting analysis based on the A-site and B-site doping fractions. As shown in Figure S3(a), a linear fitting correlation (Eq. (1-1)) resulted in a statistical R^2 value of 0.7290. However, it was observed from experiments that excessive cobalt doping led to a reduction in sorption capacity. Consequently, we employed a non-linear fitting correlation (Eq. (1-2)), which yielded a higher R^2 value of 0.8510. It is clearly indicated that, for the $Sr_xBa_{1-x}Fe_yCo_{1-y}O_{3-\delta}$ perovskites, the impact of B-site doping outweighed that of A-site doping. For the $Sr_xBa_{1-x}Fe_yMn_{1-y}O_{3-\delta}$ perovskites, the linear fitting also achieved a substantial R^2 value of 0.8872.

$$SC = 7.0992 - 0.4123\,(1-x) + 46.9698\,(1-y) \tag{1-1}$$

$$SC = 5.6242 - 18.4125\,(1-x) + 133.2972\,(1-y) - 97.1017(1-y)^2 \tag{1-2}$$

$$SC = -7.9051 + 18.8008\,(1-x) + 68.7125\,(1-y) \tag{1-3}$$

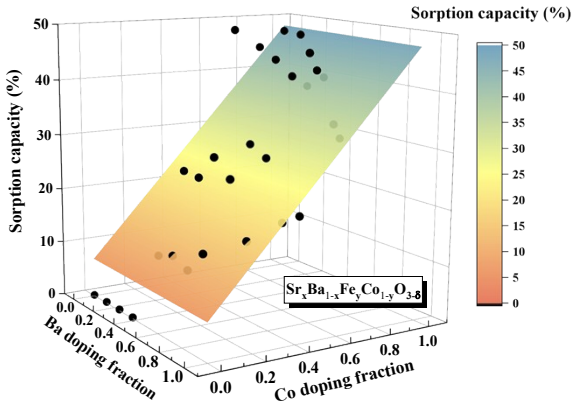

(a)

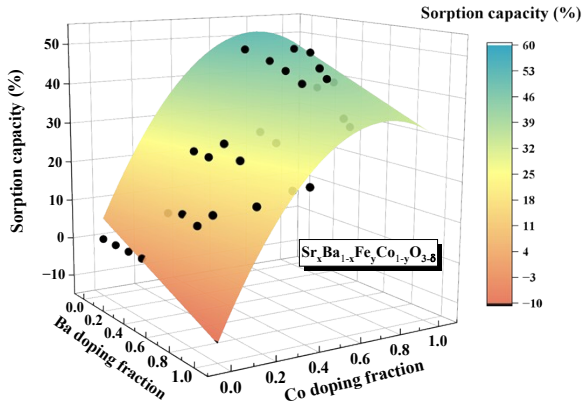

(b)

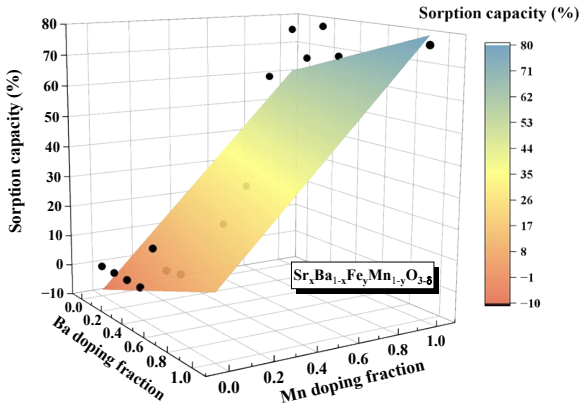

(c)

Figure S3. Fitting results between the doping fractions of A-site and B-site elements and the sorption capacity. (a) linear fitting of $Sr_xBa_{1-x}Fe_yCo_{1-y}O_{3-\delta}$; (b) non-linear fitting of $Sr_xBa_{1-x}Fe_yCo_{1-y}O_{3-\delta}$; (c) linear fitting of $Sr_xBa_{1-x}Fe_yMn_{1-y}O_{3-\delta}$

Additionally, to identify an effective correlation for predicting CO_2 capacity, we first conducted a preliminary examination on the independence of three fitting variables, ΔG_{syn}, ΔG_{abs}, and ΔG_{reg}. The correlations between ΔG_{syn} and ΔG_{abs}, ΔG_{syn} and ΔG_{reg}, and ΔG_{abs} and ΔG_{reg} are 0.7676, -0.5870, and -0.8022, respectively. Thus, we can consider them as three independent variables for fitting purposes. The fitting correlations and their corresponding statistical R^2 values are provided in Table S3 for reference.

Table S2. Fitting results between the sorption capacity and different descriptors

Fitting equation	R^2	Equation number
$SC = -172.5190 * (\Delta G_{abs} + \Delta G_{reg}) - 24.2130$	0.7649	(2-1)
$SC = 50.3100 + 45.1591 * \Delta G_{syn}$	0.0711	(2-2)
$SC = 51.4505 + 144.5702 * \Delta G_{abs}$	0.1817	(2-3)
$SC = 10.8055 - 112.2743 * \Delta G_{reg}$	0.6389	(2-4)
$SC = 46.3083 - 24.9376 * \Delta G_{abs} + 182.9161 * \Delta G_{reg}$	0.1906	(2-5)
$SC = -15.8277 - 52.3066 * \Delta G_{syn} - 137.7448 * \Delta G_{reg}$	0.7014	(2-6)
$SC = -30.0746 - 204.5265 * \Delta G_{abs} - 180.2220 * \Delta G_{reg}$	0.7685	(2-7)
$SC = -31.7904 - 9.7560 * \Delta G_{syn} - 188.2580 * \Delta G_{abs} - 179.5680 * \Delta G_{reg}$	0.7698	(2-8)

5. Detailed demonstration results of methane, biogas and biomass

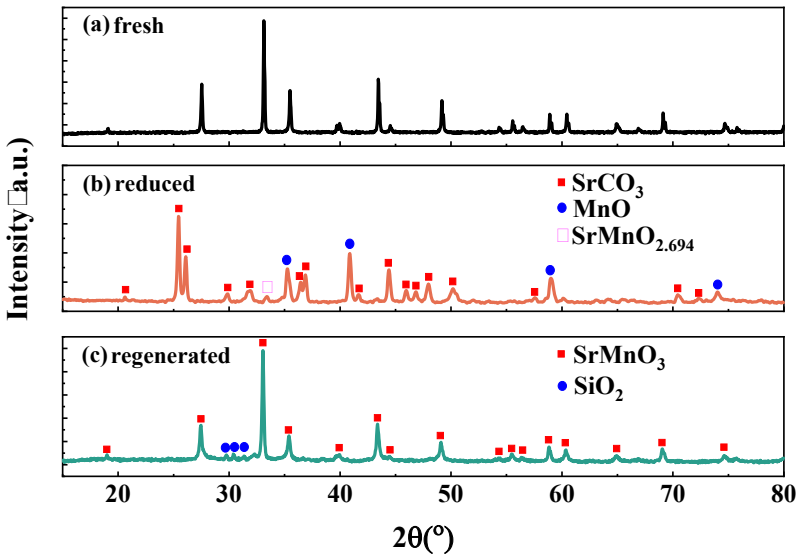

Figure S4. XRD patterns of samples from the sorption-enhanced biogas reforming experiments. (a) fresh sample; (b) reduced sample; (c) regenerated sample after 20 cycles. The presence of SiO_2 in the sample could originate from the inert packing material of quartz wool or the reactor wall of the quartz U-tube

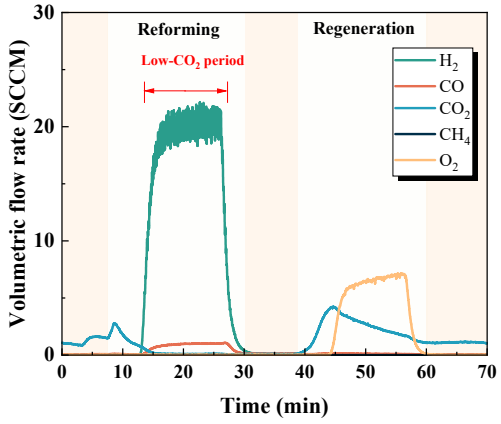
Reforming
Regeneration
Low-CO2 period
H2
CO
CO2
CH4
O2
Volumetric flow rate (SCCM)
Time (min)

(a)

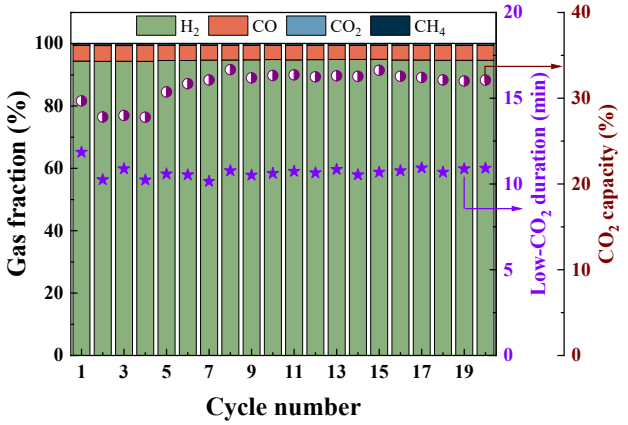
H2
CO
CO2
CH4
Gas fraction (%)
Low-CO2 duration (min)
CO2 capacity (%)
Cycle number

(b)

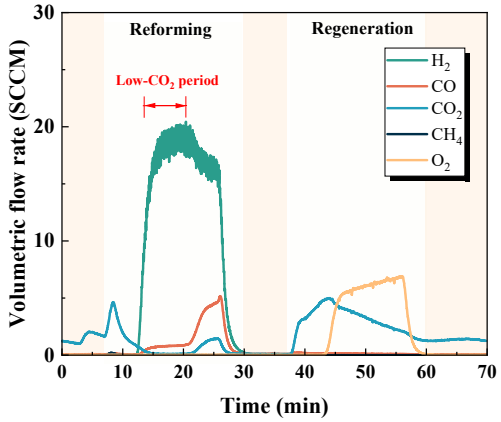
Reforming
Regeneration
Low-CO2 period
H2
CO
CO2
CH4
O2
Volumetric flow rate (SCCM)
Time (min)

(c)

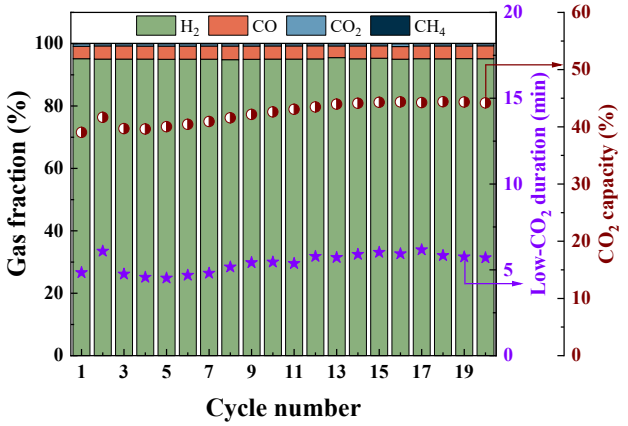
H2
CO
CO2
CH4
Gas fraction (%)
Low-CO2 duration (min)
CO2 capacity (%)
Cycle number

(d)

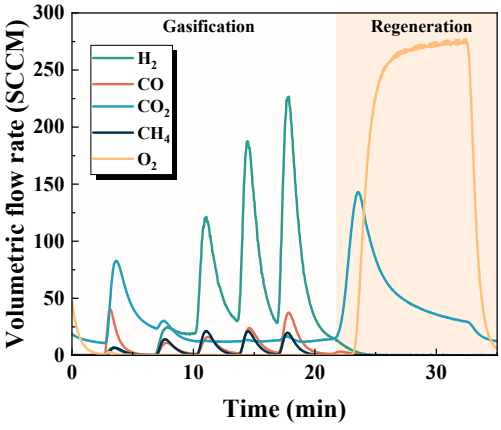
Gasification
Regeneration
H2
CO
CO2
CH4
O2
Volumetric flow rate (SCCM)
Time (min)

(e)

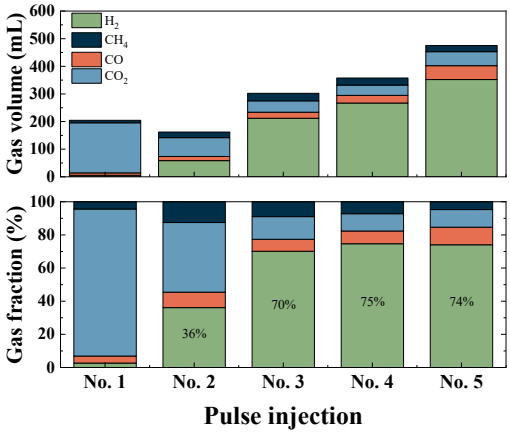
H2
CH4
CO
CO2
Gas volume (mL)
Gas fraction (%)
36%
70%
75%
74%
No. 1
No. 2
No. 3
No. 4
No. 5
Pulse injection

(f)

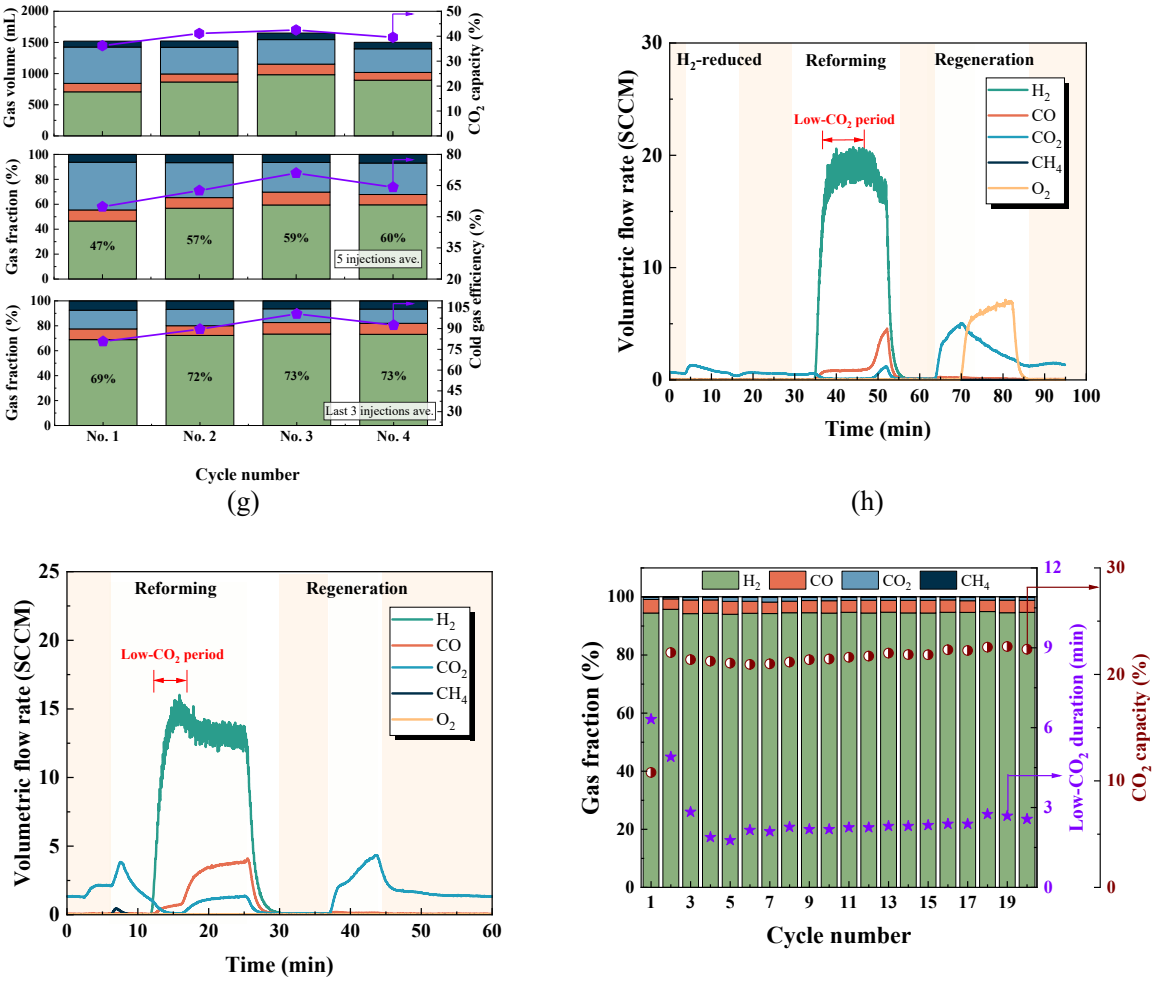

Figure S5 Reactor performance results. Sorption-enhanced steam reforming of methane (a, b), biogas(c, d), sorption-enhanced gasification of biomass (e, f, g), and sorption-enhanced steam reforming of biogas with H_2 pre-reduction (h) and partial regeneration (i, j). (a, c, e, h, and i): typical product profiles measured by online MS. (b, d, and j): Low-CO_2 duration, sorption capacity, and dry-basis and Ar-free concentrations of gaseous products during the low-CO_2 period over 20 cycles. (f): dry-basis and Ar-free concentrations of gaseous products and their gas volumes in five different pulse injections; (g): sorption capacity, total gas volume, average gaseous concentrations, and cold gas efficiencies of five injections and average gaseous concentrations of last three injections over four cycles.

6. Life-cycle assessment

The goal of this simplified life-cycle assessment is to evaluate the global house gas (GHG) emissions associated with hydrogen production through the sorption-enhanced reforming of biogas (SERB). As illustrated in Figure S4, the functional units considered in this study included a biogas production plant, a sulfur removal unit, a SERB plant, a hydrogen purification system, a carbon sequestration system, and a cryogenic air separation plant. In this process, after the removal of H_2S, the biogas is directed to the SERB plant to produce hydrogen with a purity up to 95%. Subsequently, a hydrogen purification system is employed to further increase the hydrogen concentration for downstream applications. Additionally, 99% pure oxygen generated by the cryogenic air separation plant is used to initiate the release of pure CO_2. The captured CO_2 is then compressed to 150 bar and transported via a pipeline to a nearby underground storage site for carbon sequestration.

Given its developmental stage, it is difficult to accurately estimate the CO_2 emissions during the construction phase. However, previous studies have indicated that CO_2 emissions related to equipment manufacturing and construction constitute only a minor percentage of the total emissions in a chemical looping power plant [1,2]. Additionally, previous studies also indicated that oxygen carriers and catalysts contribute only a small percentage to the global warming potential (GWP) during the adequate operational lifetime [1,3]. Consequently, the GWP associated with plant construction and catalyst manufacturing was not included in our current LCA study. The CO_2 leakage during piping and sequestration is also assumed to be negligible compared to the large quantity of CO_2 stored.

The amount of O_2 necessary for sorbent regeneration and decarbonation plays a crucial role in defining the energy requirements for O_2 production. Consequently, the oxygen consumption rate is specified by Eq. (3). The composition of the raw biogas is assumed to be 60% CH_4, 35% CO_2, 4.7% H_2O, and 0.3% H_2S. The global warming potential (GWP) of each functional unit is summarized in Table. S3. The hydrogen yield and CO_2 capture efficiency were determined based on the performance results during the low-CO_2 period (as shown in Figure S4(i/j)). They can be obtained by Eqs. (4-5):

$$O_2\ consumption\ rate = \frac{n_{O_2,feed}}{n_{CO_2,release}} \quad (3)$$

$$H_2\ yield = \frac{n_{H_2,produced}}{n_{CH_4,feed}} \quad (4)$$

$$\eta_{CO_2\ capture} = \frac{n_{CH_4,feed} + n_{CO_2,feed} - n_{COx,observed}}{n_{CH_4,feed}} \quad (5)$$

The total GHG emissions are estimated to be approximately -2.18 kg CO_2eq per kg of H_2 produced, signifying a net reduction in GHG emissions. We also explored a scenario involving the recycling of exhaust gas from the purification unit back to the reforming reactor. Assuming a typical hydrogen recovery efficiency of 0.9, the actual hydrogen yield decreased to 3.15 mol H_2/mol CH_4. Consequently, the corresponding GHG emissions would decrease to -2.42 kg CO_2eq/kg $_{H2}$, as more CO_2 would be captured in the production of 1 kg of hydrogen. However, we have chosen to report the more conservative value in our paper.

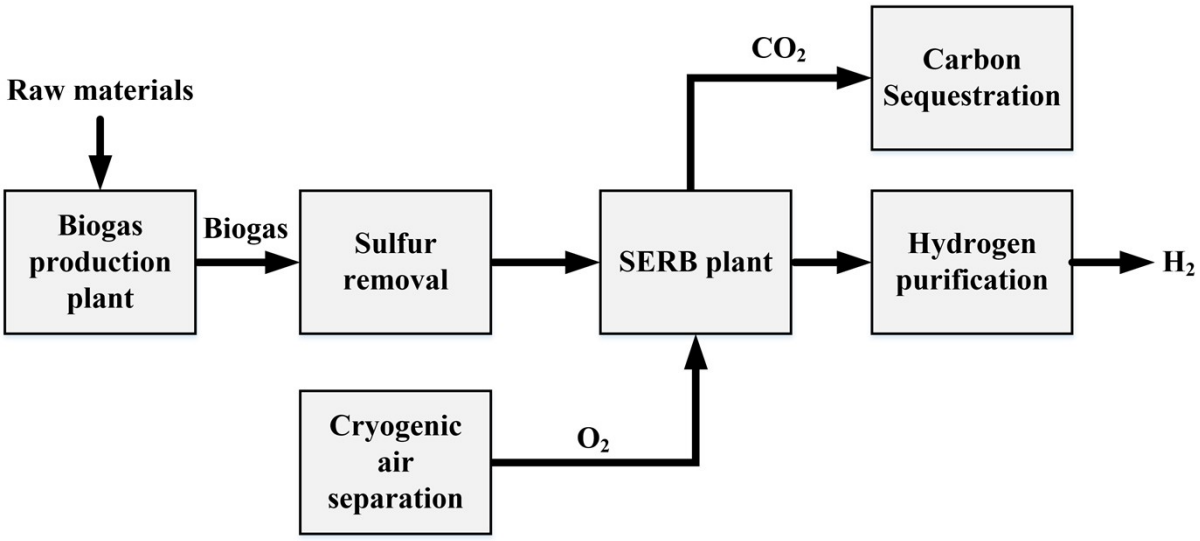

Figure S6. System boundary of hydrogen production through the sorption-enhanced reforming of biogas (SERB) process

Table S3. GWP of each functional unit and the relevant key parameters for the LCA calculation

Subsystem	Items	Unit	Value	Reference
Biogas production plant	GWP	kg CO_2eq/mol CH_4	0.02788	[4]
Sulfur removal	GWP	kg CO_2eq/kg H_2S	13.9	[5]
	GWP	kg CO_2eq/mol CH_4	0.002363	
Oxygen separation	Electricity consumption	kWhe/ton O_2	300	[6]
	GWP	g CO_2 eq/kWhe	600	[7]
	GWP	kg CO_2eq/mol O_2	0.01025	Calculation
Hydrogen purification	GWP	kg CO_2eq/mol CH_4	0.000311	[4]
SERB plant	Hydrogen yield	mol H_2/mol CH_4	3.5	Experiment
	Oxygen consumption rate	mol O_2/mol CO_2	1.29	
	CO_2 capture efficiency	mol CO_2/mol CH_4	1.38	
	GWP	kg CO_2eq/mol CH_4	-0.06072	Calculation
Carbon sequestration	CO_2 compression	kWhe/kgCO_2	0.116	[8]
	CO_2 transport	kWhe/kgCO_2	0.005	[9]
	CO_2 injection	kWhe/kgCO_2	0.007	[9]
	GWP	kg CO_2eq/mol CH_4	0.0046	Calculation
Total	GWP	kg CO_2eq/mol CH_4	-0.0199	Calculation
	GWP	kg CO_2eq/kg H_2	-2.18	

7. Detailed methodology

7.1 The approach to calculate the sorption capacity in the TGA

We assumed the oxygen uptake rate far surpassed the decarbonation rate. As a result, the initial weight gain observed during the regeneration step could be attributed solely to oxygen uptake. The separated B-site metal oxides were assumed to be oxidized to Mn_2O_3, Co_3O_4, NiO, CuO, and Fe_2O_3. Furthermore, based on this assumption, the perovskite material would promptly reform following the decarbonation process in the regeneration step. The corresponding observed weight loss was the net weight change between the CO_2 release and oxygen uptake. The CO_2 sorption capacity can be calculated by Eq. (6).

$$SC=\left(\frac{m_1}{MW_{CO_2}}+\frac{m_2}{MW_{CO_2}-\delta_1 MW_{\mathrm{O}}}\right)\div\left(\alpha\cdot\frac{m_{reduced}}{MW_{reduced}}\right) \quad (6)$$

As illustrated in Figure S7, m_1 and m_2 are the weight losses at the second purge step and the regeneration step, respectively. MW_{CO2} is the molar mass of CO_2 molecule, and $MW_{reduced}$ is the reduced perovskite mixture. δ_1 represents the number of oxygen atoms absorbed by the B-site metal during the weight loss period in the regeneration step. For example, Co_3O_4 absorbs 0.63 oxygen atom when fully regenerated into the valence state of B-site in $SrCoO_{2.8}$. α is the weighted ratio representing the theoretical maximum CO_2 capacity of A-site elements. Ca, Sr, and Ba can absorb CO_2 with a ratio of 1:1, while K can only absorb CO_2 with a ratio of 0.5:1. The method for calculating CO_2 capacity reported in our previous study [10] represents a specific instance of Eq.(6), which δ_1 is approximately 0 (Brownmillerite phase) while α is 1.

The oxygen capacity can be calculated by Eq. (7).

$$OC=\left(\frac{m_3}{MW_O}+\frac{m_2\cdot\delta_1 MW_O}{MW_{CO_2}-\delta_1 MW_{\mathrm{O}}}\right)\div\left(\frac{m_{reduced}}{MW_{reduced}}\right) \quad (7)$$

Where m_3 is the weight gain at the beginning of regeneration step, MW_O is the molar mass of O atom.

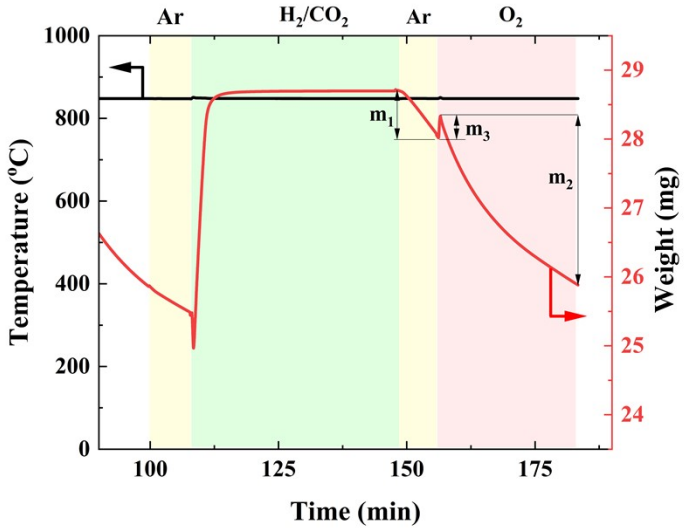

Figure S7. A typical TGA experiment for measuring the sorption capacity and oxygen capacity of the perovskite oxide

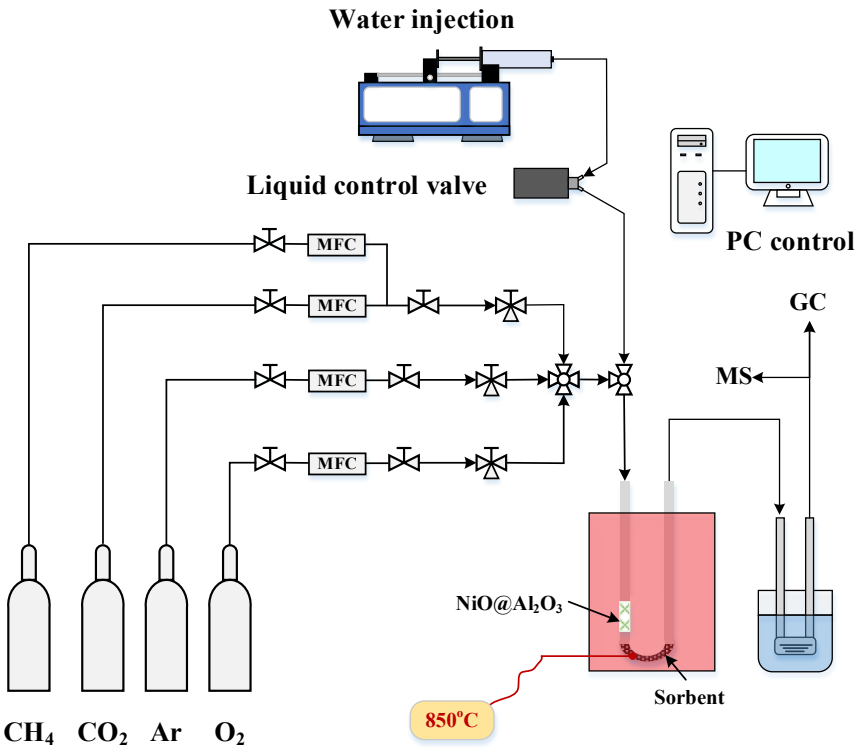

Figure S8. Schematics of the packed bed reactor system for the sorption-enhanced steam reforming of methane and biogas

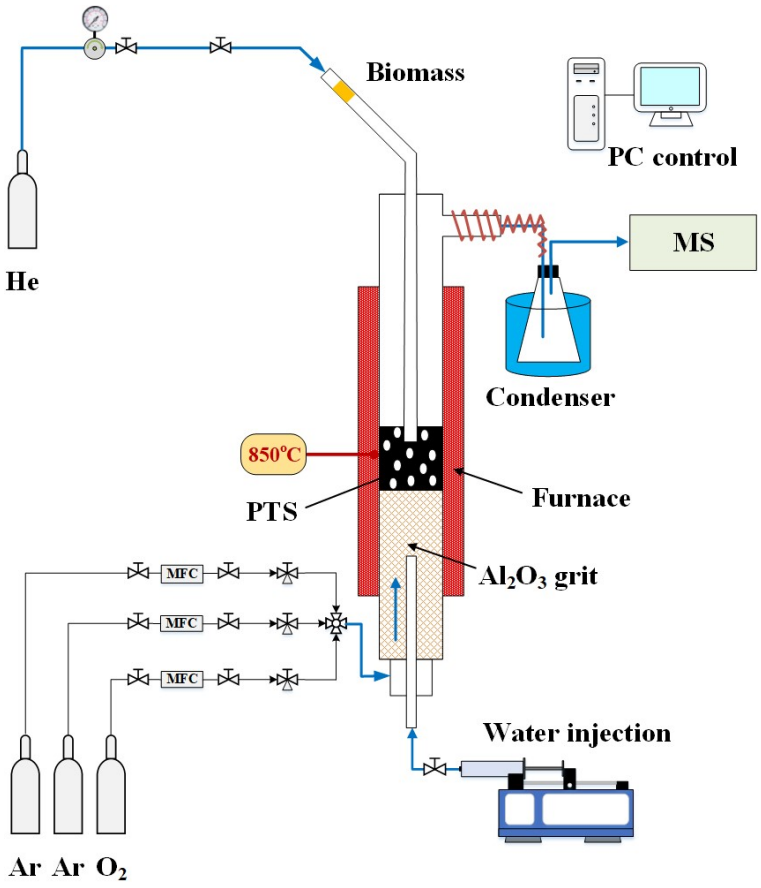

Figure S9. Schematics of the bubbling fluidized bed reactor

Table S4. The proximate and ultimate analyses of as-received biomass used for the tests of sorption-enhanced gasification of biomass

Parameter	M_{ar}*	A_{ar}	V_{ar}	C_{daf}**	H_{daf}	N_{daf}	O_{daf}	LHV_{ar}
Unit	%	%	%	%	%	%	%	MJ/kg
Value	5.34	2.3	77.6	50	6.2	0.1	43.7	15.55

*: as received samples

**: dried ash-free samples

References:

[1] Fan, J., Hong, H. & Jin, H. Life cycle global warming impact of CO_2 capture by in-situ gasification chemical looping combustion using ilmenite oxygen carriers. *J. Clean. Prod.* **234**, 568-578, (2019).

[2] Fan, J., Hong, H. & Jin, H. Power Generation Based on Chemical Looping Combustion: Will it qualify to reduce greenhouse gas emissions from life-cycle assessment? *ACS Sustain. Chem. Eng.* **6**, 6730-6737, (2018).

[3] Navajas, A. et al. Life cycle assessment of natural gas fuelled power plants based on chemical looping combustion technology. *Energy Convers. Manage.* **198**, 111856, (2019).

[4] Hajjaji, N., Martinez, S., Trably, E., Steyer, J.-P. & Helias, A. Life cycle assessment of hydrogen production from biogas reforming. *Int. J. Hydrogen Energy* **41**, 6064-6075, (2016).

[5] Cano, P. I. et al. Life cycle assessment of different physical-chemical and biological technologies for biogas desulfurization in sewage treatment plants. *J. Clean. Prod.* **181**, 663-674, (2018).

[6] Dong, X., Wang, B., Yip, H. L. & Chan, Q. N. CO_2 emission of electric and gasoline vehicles under various road conditions for China, Japan, Europe and world average—prediction through Year 2040. *Appl. Sci.* **9**, 2295, (2019).

[7] Mehrpooya, M., Golestani, B. & Ali Mousavian, S. M. Novel cryogenic argon recovery from the air separation unit integrated with LNG regasification and CO_2 transcritical power cycle. *Sustain. Energy Technol. Assess.* **40**, 100767, (2020).

[8] Rochelle, G. *et al.* Aqueous piperazine as the new standard for CO_2 capture technology. *Chem. Eng. J.* **171**, 725-733, (2011).

[9] Chisalita, D.-A. *et al.* Assessing the environmental impact of an integrated steel mill with post-combustion CO_2 capture and storage using the LCA methodology. *J. Clean. Prod.* **211**, 1015-1025, (2019).

[10] Brody, L. et al. Perovskite-based phase transition sorbents for sorption-enhanced oxidative steam reforming of glycerol. *ACS Sustain. Chem. Eng.* **10**, 6434-6445, (2022).